RSC Advances

PAPER

View Article Online
View Journal | View Issue

Cite this: *RSC Adv.*, 2021, **11**, 35489

Catalytic effect of laser-combined atmospheric pressure plasma in lowering the reduction temperature of hematite†

Jaemin Yoo, [a] Dongkyu Lee, [b] Jimo Lee, [a] Taehyeong Kim, [b] Hyungyu Jin *[b] and Gunsu S. Yun *[acd]

Received 13th September 2021
Accepted 25th October 2021

DOI: 10.1039/d1ra06858j

rsc.li/rsc-advances

Atmospheric pressure plasma (APP) generates highly reactive species that are useful for surface activation. We demonstrate a fast regeneration of iron oxides, that are popular catalysts in various industrial processes, using microwave-driven argon APP under ambient conditions. The surface treatment of hematite powder by the APP with a small portion of hydrogen (0.5 vol%) lowers the oxide's reduction temperature. A near-infrared laser is used for localized heating to control the surface temperature. Controlled experiments without plasma confirm the catalytic effect of the plasma. Raman, XRD, SEM, and XPS analyses show that the plasma treatment changed the chemical state of the hematite to that of magnetite without sintering.

Introduction

The capability of exchanging oxygen in metal oxides *via* thermochemical redox reactions has led to production of gas fuels like carbon monoxide, hydrogen, or syngas, as well as to storage of thermal energy in matter.[1–3] The oxygen exchange starts when metal oxides absorb enough heat to lose their lattice oxygen and subsequently release oxygen gas to the environment. Next, the reduced oxides are reoxidized by various oxidants like CO_2, H_2O, and O_2 to produce gas fuels. Such thermochemical reactions can be improved when the material has a large extent of oxygen exchange. That is to say, materials having a large redox capacity can produce a larger amount of gas fuel and store more energy.

Iron oxides are a promising system for redox catalysis due to the low third ionization potential compared to other non-stoichiometric metal oxides. Despite the potentially large redox capacity the iron oxide has, its rapid sintering and high reduction temperature have hindered practical use in fuel production or energy storage.[1,4] The high reduction temperature leads to durability issues in the reactor wall materials as well as significant heat loss during redox cycles. The latter requires the use of additional components for heat recovery to enhance the system efficiency.[5–7]

Integrating plasma with thermochemical redox reactions is expected to result in multiple synergistic effects that can address the above issues. First, applying plasma on metal oxide catalysts including iron oxides can significantly reduce the reduction temperature, which could alleviate both the durability and heat loss issues. Plasma offers an exceptional advantage in making radicals such as ro-vibrationally or electronically excited molecules, ions, and neutral species which are highly reactive for various chemical reactions.[8,9] Such abundant radicals acting on reactants can lower the activation barrier due to their high reactivity[10] or change the reaction pathway[9,11] in chemical reactions. In addition, the absorption of plasma-generated electrons is expected to facilitate the loss of lattice oxygen and the subsequent re-distribution of electron charge in metal oxides.[12,13] Those rich effects of plasma on both reactants and metal oxide catalysts could reduce the reduction temperature or enhance the reaction kinetics at a given temperature.[8,14] Second, plasma can induce a self-heating effect in the applied catalyst sample, which considerably diminishes the heating demand for the reactor. As the self-heating effect is confined to the impacted sample volume, the sample can reach a required temperature with much less energy consumption compared to that in a conventional reactor system. In some cases, it is even expected that no additional heating is necessary other than that provided by the self-heating. The above-mentioned advantages make integrating plasma an attractive method to realizing a highly efficient thermochemical redox system.

Much attention has recently been given to atmospheric pressure plasma (APP) for its high plasma density and convenient operation in an open space without the need for a bulky chamber. While APP can be discharged with various power

[a]*Division of Advanced Nuclear Engineering, Pohang University of Science and Technology, Pohang, 37673, Republic of Korea. E-mail: gunsu@postech.ac.kr*

[b]*Department of Mechanical Engineering, Pohang University of Science and Technology, Pohang, 37673, Republic of Korea. E-mail: hgjin@postech.ac.kr*

[c]*Department of Physics, Pohang University of Science and Technology, Pohang, 37673, Republic of Korea*

[d]*Max Planck Center for Attosecond Science, Max Planck POSTECH/Korea Research Initiative, Pohang, 37673, Republic of Korea*

† Electronic supplementary information (ESI) available. See DOI: 10.1039/d1ra06858j

sources, ranging from DC to GHz, a microwave is particularly known for its highly effective confinement of electrons combined with high displacement current, generating energetic electrons and promoting higher production rates of reactive species.[15–21] Some other characteristics of microwave-driven plasma include low voltage/power operation, long lifetime electrode, and low production of ozone.[16,17,22,23]

In the current work, we report a catalytic effect of APP in lowering the temperature required for the reduction of hematite using a compact microwave-driven plasma jet source called a Coaxial Transmission Line Resonator (CTLR).[15] A very small amount of hydrogen, an intense reducing agent, and a near-infrared laser (808 nm) under continuous wave mode for localized heating are used to enhance the rate of reduction process. The microwave plasma has non-thermal properties (electron temperature ≫ gas temperature),[24,25] hence surface heating by plasma is limited to an order of hundreds Kelvin. Accordingly, we combine the near-infrared laser capable of providing rapid local surface heating, for the purpose of facilitating system temperature control while minimizing the thermal effect of the plasma. In that regard, our approach of combining laser and plasma could be catalytically more effective compared to plasma alone[25,26] or laser alone process.[27] Also, it provides a platform to investigate the catalytic effects of plasma by separating the thermal effect. More details of the experimental setup can be found in ESI (Fig. S1†).

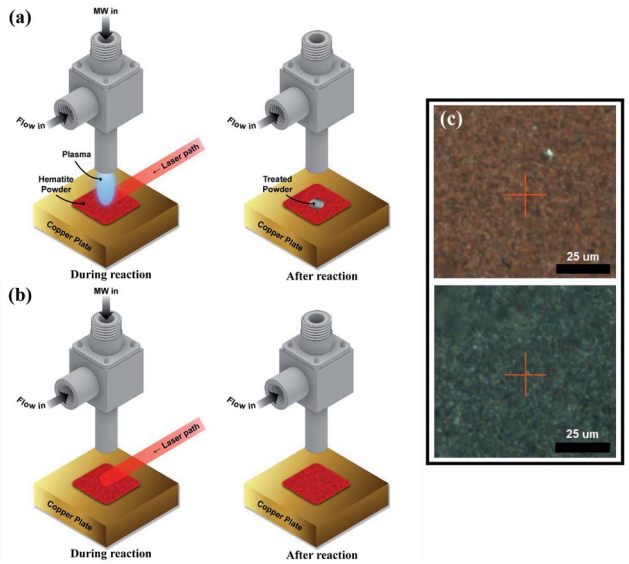

Fig. 1 Reaction processes of (a) both plasma and laser on and (b) laser on only, and (c) microscopic images of untreated hematite (top) and plasma-treated hematite (bottom). In the laser-only case (b), the gas flow and microwave (MW) power are the same as in (a). The red cross marks in the microscopic images of (c) indicate the location of Raman spectroscopy measurement. The 'flow in' gas composition of (a) and (b) are both argon mixed with 0.5 vol% hydrogen.

Results and discussion

The laser-combined plasma treatment shows that the presence of plasma helps the chemical reaction in the reduction of the hematite. The surface of the hematite starts to reduce at the radiation temperature (T_{rad}) of about 570 K in the plasma-laser combined condition. The laser only condition, however, requires a much higher T_{rad} of about 720 K for the surface to be reduced. Fig. 1a and b show two different combinations of plasma and laser irradiation on the hematite surface at $T_{rad} \approx$ 630 K, and 5 minute irradiation for each combination is performed to ensure sufficient reaction. In both cases, the surface temperature is instantly reached 630 K from room temperature by the laser heating. Under such conditions, dramatic color change on the surface is observed in 1a case, whereas no distinct change is detected with the laser-only case as shown in Fig. 1b. These results suggest the probable catalytic effect of plasma on hematite powder, that is, lowering the reduction energy barrier of metal oxides. We consider three possible factors for the observation: microwave heating, abundant energetic electrons, and hydrogen reactive species. A few studies on thermochemical redox reactions *via* microwave heating have been reported.[12,28,29] The studies showed that the direct radiation of microwave can promote the loss of lattice oxygen on metal oxides. The microwave-driven plasma introduced in the current work, however, is positioned far from the surface. The heating effect of microwave is thus negligible. Abundant electrons generated by the plasma are presumed to be the main factor of low reduction temperature as electrons play a major role in the formation of polarons and oxygen vacancies in metal oxides.[12] It was shown that negative surface charging by electrons, in terms of chemisorption, can increase the reductive capabilities in the reduction of CO_2, suggesting an electron-induced synergistic effect in plasma catalysis.[13] It is thus conceivable that the induced negative charge on the surface can promote the reduction of metal oxides. As a small portion of hydrogen (0.5%) mixed with argon is used for the plasma discharge, reactive hydrogen species (H_2^*, H^+, H *etc.*) cannot be neglected. In particular, H_2^* (ro-vibrationally excited hydrogen molecule) is the dominant radical species in microwave-induced non-thermal hydrogen plasma and can assist the reduction process of metal oxides.[14,30,31]

As mentioned earlier, combining the high reactivity of microwave plasma and the fast surface heating by laser offers several advantages in terms of the energy efficiency and time scale of catalytic reactions compared to the laser or plasma alone case. The main advantage of using laser as a heating source is the acceleration of reaction rate by compensating for the insufficient local heating capability of plasma. The rapid heating by laser can minimize undesired reactions as well as prevent the destruction of the target. Laser heating is also more energy-efficient than convection heating, as it can significantly reduce massive heat loss from the reactor to the environment or to the process gases.

The observed change on the hematite surface is analyzed using a Scanning Electron Microscope (SEM), an X-ray Diffractometer (XRD), a Raman spectrometer, and an X-ray Photoelectron Spectrometer (XPS).

We analyzed the morphological changes of the hematite powder sample by SEM before and after the plasma treatment.

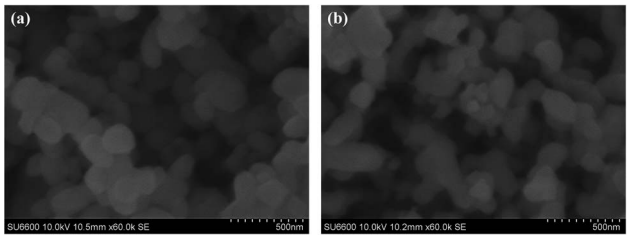

Fig. 2 SEM images of (a) untreated hematite and (b) plasma-treated hematite for 5 minute.

Fig. 2 shows that the untreated hematite particles have the average size under 500 nm, and the size of particle is maintained after the 5 minute plasma treatment without sintering. This finding implies that the plasma treatment is a suitable technique for reducing metal oxides without damages.

Fig. 3 shows the diffraction patterns of untreated and plasma-treated hematite samples. It is noted that the patterns contain both signals from the surface and the bulk of the sample as the XRD measures bulk diffraction patterns. The measured patterns were analyzed using the Rietveld refinement method[32] to quantify the volumetric fraction of hematite and magnetite. The detail of the method is described in Fig. S2 and Table S1 in the ESI.† Miller index planes obtained from the Inorganic Crystal Structure Database (ICSD) are indicated. The Miller indices denoted by (012), (104), (111), (113), (024), (116), (122), (214) and (300) correspond to a reference hematite sample (ICSD code 01-080-5407 and 01-089-8103).[33] The Miller indices denoted by (111), (220), (202) and (511) correspond to a reference magnetite sample (ICSD code 01-071-6336 and 01-076-2949).[33,34] Fig. 3 shows that the plasma treatment has partially changed the chemical state of hematite to that of magnetite. In addition, the weakening of the signal intensity of the treated hematite indicates that the treated sample has a state of the 2-phase mixture (hematite–magnetite). The observation of a fine shift in main peaks, (111), is an evidence of phase shift.

We use Raman spectroscopy for cross-validation of the XRD results, and X-ray Photoelectron Spectroscopy (XPS) for assessment of the chemical state of the sample surfaces. Fig. 4a

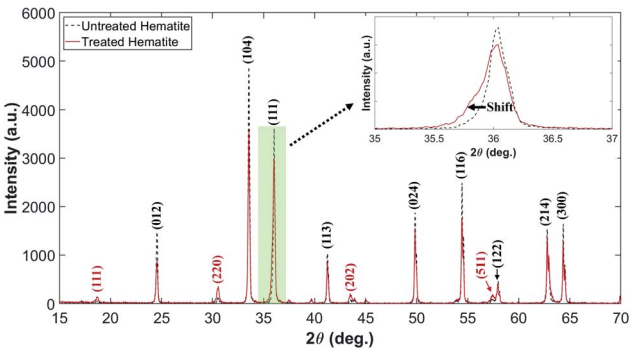

Fig. 3 XRD patterns of untreated and plasma-treated hematite samples. The pale green box is magnified to discern the shift clearly.

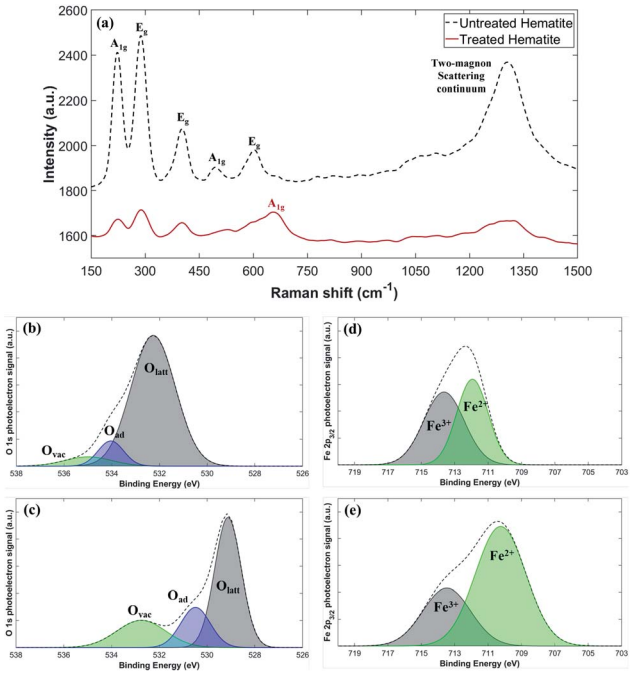

Fig. 4 (a) Raman and (b–e) photoelectron spectra collected from the untreated and plasma-treated hematite samples. (b) O 1s for the untreated hematite, and (c) O 1s for the plasma-treated hematite. (d) Fe $2p_{3/2}$ for the untreated, and (e) Fe $2p_{3/2}$ for the plasma-treated hematite. O_{latt}, O_{ad}, and O_{vac} mean lattice oxygen, adsorbed oxygen (surface oxygen in the –OH or H_2O form), and oxygen vacancy (oxygen-deficient environment with O^{2-} vacancies), respectively.

presents the Raman spectra of untreated and plasma-treated hematite samples. The observed peaks at A_{1g} and E_g for the untreated sample correspond to the phonon vibrational mode of hematite, and the continuum signal appearing near 1318 cm^{-1} corresponds to the two-magnon scattering of hematite.[35,36] The A_{1g} peak near 668 cm^{-1} for the plasma-treated sample corresponds to the vibrational mode of magnetite.[37,38] The partially weakened hematite peaks and A_{1g} of magnetite peak show that the plasma-treated hematite has a state of the two-phase mixture, which is consistent with the XRD results.

The surface electronic state of the samples is analyzed by XPS. While the O_{latt} peak is a representative peak for typical metal–oxygen bonds, the O_{vac} peak at a higher energy is attributed to the surface oxygen vacancies. The untreated sample has a small O_{vac} peak at the binding energy slightly above 534 eV (Fig. 4b), but the plasma-treated sample shows a much larger O_{vac} peak at a slightly lower energy resulting in the high peak asymmetry (Fig. 4c).[39–44] This indicates that the plasma-treated sample contains a significantly larger number of surface oxygen vacancies compared to the untreated sample. Fig. 4d and e show the representative Fe $2p_{3/2}$ peaks of the untreated and the plasma-treated samples.[45,46] Fe $2p_{3/2}$ peaks (~711 eV) exhibit multiplet characteristic wherein Fe^{2+} has a relatively lower binding energy compared to Fe^{3+}.[47] Compared to the untreated sample, the Fe $2p_{3/2}$ peaks of the plasma-treated sample show an increased signal in the lower energy around 710.3 eV indicating that some of Fe^{3+} are reduced to

Fe^{2+}, consistent with the increased number of oxygen vacancies. Specifically, the relative ratio of $Fe^{2+}/(Fe^{2+} + Fe^{3+})$ can be calculated by comparing the area under the fitted curves. The untreated sample has only 47.7% of Fe^{2+}, which increases to 70.2% after the plasma treatment. The increased area under the Fe^{2+} peak suggests that the plasma treatment effectively removes lattice oxygen in the hematite. On the other hand, the area under the Fe^{3+} peak decreases after the plasma treatment, presumably because Fe^{3+} is reduced with extra electrons supplied by plasma or by the formation of oxygen vacancies.[48,49] It may be hypothesized that in the process the high-energy electrons supplied by plasma help to break the Fe–O bonding, facilitating the oxygen gas evolution. Another possible route is that rich hydrogen radicals produced by plasma may work as an effective reducing agent. Additional electrons, generated by the creation of oxygen vacancies or supplied by plasma, are consumed by the reduction process of $Fe^{3+} + e^- \rightarrow Fe^{2+}$. Both of the oxygen vacancy generation and reduction of Fe^{3+} to Fe^{2+} could induce the lattice distortion resulting in the increase of the lattice constant. The increased lattice constant indicates loosening of the Fe–O bond, which generally shifts XPS peaks to lower energy positions. In addition, the binding energy of Fe^{2+} atoms is decreased compared to Fe^{3+} atoms due to enhanced electrostatic shielding by electrons. Such a reduction in binding energy also causes overall peak shift to lower energies in XPS. Thus, the observed overall peak shift to lower energies after the plasma treatment (Fig. 4b–e) could be attributed to either the lattice distortion or the enhanced electrostatic shielding, or both.

Conclusions

Here we proposed a novel technique for the fast control of the surface chemical state of hematite using microwave-driven atmospheric pressure plasma. SEM, XRD, Raman, and XPS analyses show that the chemical state of the hematite powder was partially changed to that of magnetite by the plasma with laser-heating under ambient pressure. The catalytic effect of microwave-driven plasma is confirmed by the unaffected surface of the control sample treated by laser only.

The reduced hematite by plasma showed the state of a partially reduced 2-phase mixture rather than the completely reduced state as metallic iron (Fe). Hematite has three well-known reduced phases: magnetite (Fe_3O_4), Wüstite ($Fe_{1-x}O$), iron (Fe). The fast control capability of the surface temperature using the laser enables the rapid reduction of hematite because the reduction rate increases with temperature.[50] The combined effect of plasma and laser surface heating also enables to reach intermediate reduced states. Hence, the proposed laser combined plasma system can provide a platform for the study of reduction and oxidation process of metal oxides.

Lowering the reduction temperature by plasma may offer significant advantages in thermochemical hydrogen production, wherein high reduction temperatures required to generate oxygen vacancies in metal oxides have been a critical bottleneck for commercialization. Lower operation temperature provides engineering benefits in system durability, the choice of heat sources, and thermal efficiency. Moreover, the non-sintering of the hematite particles after treatment in our experiments suggests that the introduction of plasma can help maintain a constant efficiency in the redox cycles.

It is noted that our experimental setup has one limitation on the temperature measurement. We choose the infrared imaging camera to indirectly measure the rapid change of the surface temperature during the treatments. However, it is difficult to track the change of the surface emissivity during the reduction reaction of hematite to magnetite, which is required for exact temperature measurement. This limits the thermodynamic analysis of the redox reaction with temperature dependence. Developing a tool to accurately measure the surface temperature of the plasma-metal oxide interface remains as a challenge.

We have presented three probable hypotheses of the low reduction temperature; effects of microwave heating, surface charging of electrons, and hydrogen radicals. Further studies of their roles are subject to future study.

Conflicts of interest

The authors declare no competing financial interests in this paper.

Acknowledgements

This work is partially supported by the BK21+ program funded by the Ministry of Education, Republic of Korea and the Korea Hydro & Nuclear Power Co., Ltd (No. 2019-TECH-17).

References

1 E. N. Coker, A. Ambrosini and J. E. Miller, *RSC Adv.*, 2021, **11**, 1493.
2 B. Bulfin, J. Vieten, C. Agrafiotis, M. Roeb and C. Sattler, *J. Mater. Chem. A*, 2017, **5**, 18951.
3 T. Nakamura, *Sol. Energy*, 1977, **19**, 467.
4 J. E. Miller, A. H. McDaniel and M. D. Allendorf, *Adv. Energy Mater.*, 2014, **4**, 1300469.
5 W. C. Chueh, C. Falter, M. Abbott, D. Scipio, P. Furler, S. M. Haile and A. Steinfeld, *Science*, 2010, **330**, 1797.
6 D. Marxer, P. Furler, J. Scheffe, H. Geerlings, C. Falter, V. Batteiger, A. Sizmann and A. Steinfeld, *Energy Fuels*, 2015, **5**, 3241.
7 Y. Hao, J. Jin and H. Jin, *Appl. Therm. Eng.*, 2020, **166**, 113600.
8 K. C. Sabat, P. Rajput, R. K. Paramguru, B. Bhoi and B. K. Mishra, *Plasma Chem*, 2014, **34**, 1–23.
9 E. C. Neyts and A. Bogaerts, *J. Phys. D: Appl. Phys.*, 2014, **47**, 224010.
10 R. R. Smith, D. R. Killelea, D. F. DelSesto and A. L. Utz, *Science*, 2004, **304**, 992–995.
11 H. L. Chen, H. M. Lee, S. H. Chen, Y. Chao and M. B. Chang, *Appl. Catal. B*, 2008, **85**, 1–9.
12 J. M. Serra, J. F. Borrás-Morell, B. García-Baños, M. Balaguer, P. Plaza-González, J. Santos-Blasco, D. Catalán-Martínez, L. Navarrete and J. M. Catalá-Civera, *Nat. Energy*, 2020, **5**, 910.

13 K. M. Bal, S. Huygh, A. Bogaerts and E. C. Neyts, *Plasma Sources Sci. Technol.*, 2018, **27**, 024001.
14 P. Rajput, K. C. Sabat, R. K. Paramguru, B. Bhoi and B. K. Mishra, *Ironmak. Steelmak.*, 2014, **41**(10), 721.
15 J. Choi, F. Iza, H. J. Do, J. K. Lee and M. H. Cho, *Plasma Sources Sci. Technol.*, 2009, **18**, 025029.
16 J. Lee, W. J. Nam, S. T. Lee, J. K. Lee and G. S. Yun, *Plasma Sources Sci. Technol.*, 2018, **27**, 075008.
17 M. U. Lee, S. Y. Jeong, I. H. Won, S. K. Sung, G. S. Yun and J. K. Lee, *Phys. Plasma*, 2016, **23**, 070704.
18 F. Iza F and J. K. Lee, *Phys. Rev. Lett.*, 2007, **99**, 075004.
19 W. J. Nam, S. T. Lee, S. Y. Jeong, J. K. Lee and G. S. Yun, *Eur. Phys. J. D*, 2017, **71**, 134.
20 K. H. Schoenbach and K. Becker, *Eur. Phys. J. D*, 2016, **70**, 29.
21 K. N. Kim, J. H. Lim, G. Y. Yeom, S. H. Lee and J. K. Lee, *Appl. Phys. Lett.*, 2006, **89**, 251501.
22 S.-J. Park, J. Choi, G. Y. Park, S.-K. Lee, Y. Cho, J. I. Yun, S. Jeon, K. T. Kim, J. K. Lee and J.-Y. Sim, *IEEE Trans. Plasma Sci.*, 2010, **38**, 1956.
23 M. U. Lee, J. Lee, J. K. Lee and G. S. Yun, *Plasma Sources Sci. Technol.*, 2017, **26**, 034003.
24 M. Moreau, N. Orange and M. G. J. Feuilloley, *Biotechnol. Adv.*, 2008, **26**, 610–617.
25 C. Tendero, C. Tixier, P. Tristant, J. Desmaison and P. Leprince, *Spectrochim. Acta, Part B*, 2006, **61**, 2–30.
26 P. K. Chu, J. Y. Chen, L. P. Wang and N. Huang, *Mater. Sci. Eng. R Rep.*, 2002, **36**, 143–206.
27 J. Kusinski, S. Kac, A. Kopia, A. Radziszewska, M. Rozmus-Gornikowska, B. Major, L. Major, J. Marczak and A. Lisiecki, *Bull. Pol. Acd. Sci.: Tech. Sci.*, 2012, **60**(4), 711.
28 Y. Gao, Y. Mao, Z. Song, X. Zhao, J. Sun, W. Wang, G. Chen and S. Chen, *Applied Energy*, 2020, **279**, 115777.
29 K. Seo, S. Jeong, T. Lim and S. Ju, *RSC Adv.*, 2018, **8**, 37958.
30 K. Hassouni, A. Gicquel, M. Capitelli and J. Loureiro, *Plasma Sources Sci. Technol.*, 1999, **8**, 494–512.
31 Y. A. Mankelevich, M. N. R. Ashfold and J. Ma, *J. Appl. Phys.*, 2008, **104**, 113304.
32 S. Grazulis, D. Chateigner, R. T. Downs, A. F. T. Yokochi, M. Quiros, L. Lutterotti, E. Manakova, J. Butkus, P. Moeck and A. L. Bail, *J. Appl. Crystallogr.*, 2009, **42**, 726–729.
33 J. P. Gaviria, A. Bohe, A. Pasquevich and D. M. Pasquevich, *Physica B*, 2007, **389**, 198–201.
34 J. Xu, H. Yang, W. Fu, K. Du, Y. Sui, J. Chen, Y. Zeng, M. Li and G. Zou, *J. Magn. Magn. Mater.*, 2007, **309**, 307–311.
35 I. V. Chernyshova, M. F. Hochella Jr and A. S. Madden, *Phys. Chem. Chem. Phys.*, 2007, **9**, 1736.
36 T. P. Martin, R. Merlin, D. R. Huffman and M. Cardona, *Solid State Commun.*, 1977, **22**, 565.
37 O. N. Shebanova and P. Lazor, *J. Solid State Chem.*, 2003, **174**, 424–430.
38 D. L. A. Faria, S. Silva and M. T. Oliveira, *J. Raman Spectrosc.*, 1997, **28**, 873.
39 G. F. Moreira, E. R. Pecanha, M. B. M. Monte and L. S. L. Filho, *Miner. Eng.*, 2017, **110**, 96–103.
40 A. T. Kozakov, K. A. Guglev, V. V. Ilyasov, I. V. Ershov, A. V. Nikol'skii, V. G. Smotrakov and V. V. Eremkin, *Phys. Solid State*, 2011, **53**(1), 41–47.
41 L. Liardet, J. E. Katz, J. Luo, M. Gratzel and X. Hu, *J. Mater. Chem. A*, 2019, **7**, 6012–6020.
42 L. Xu, Q. Jiang, Z. Xiao, X. Li, J. Huo, S. Wang and L. Dai, *Angew. Chem.*, 2016, **128**, 5363–5367.
43 Y. Yang, Y. Jin, H. He and Z. Ye, *CrystEngComm*, 2010, **12**, 2663–2665.
44 M. Tou, R. Michalsky and A. Steinfeld, *Joule*, 2017, **1**, 146–154.
45 Y. Zhang, K. Dong, Z. Liu, H. Wang, S. Ma, A. Zhang, M. Li, L. Yu and Y. Li, *Prog. Nat. Sci.*, 2017, **27**(4), 443–451.
46 R. Zhang, L. Yang, X. Huang, T. Chen, F. Qu, Z. Liu, G. Du, A. M. Asiri and X. Sun, *J. Mater. Chem. A*, 2017, **5**, 12086.
47 A. P. Grosvenor, B. A. Kobe, M. C. Biesinger and N. S. McIntyre, *Surf. Inter. Anal.*, 2004, **36**, 1564–1574.
48 A. Sarkar and G. G. Khan, *Nanoscale*, 2019, **11**, 3414–3444.
49 B. Bharti, S. Kumar, H.-N. Lee and R. Kumar, *Sci. Rep.*, 2016, **6**, 32355.
50 D. Spreitzer and J. Schenk, *Steel Res. Int.*, 2019, **90**, 1900108.